Bioactive Materials 24 (2023) 551–562

Contents lists available at ScienceDirect

Bioactive Materials

journal homepage: www.keaipublishing.com/en/journals/bioactive-materials

Artificial cilia for soft and stable surface covalent immobilization of bone morphogenetic protein-2

Qi Gan [a,b], Lina Chen [a], Ho-Pan Bei [c], Sze-Wing Ng [a], Han Guo [d], Guoqiang Liu [a], Hao Pan [b], Changsheng Liu [b,*], Xin Zhao [c,**], Zijian Zheng [a,e,***]

[a] Laboratory for Advanced Interfacial Materials and Devices, School of Fashion and Textiles, The Hong Kong Polytechnic University, Kowloon, 99077, Hong Kong Special Administrative Region of China
[b] Key Laboratory for Ultrafine Materials of Ministry of Education, School of Materials Science and Engineering, East China University of Science and Technology, Shanghai, 200237, PR China
[c] Department of Biomedical Engineering, The Hong Kong Polytechnic University, Hung Hom, Hong Kong Special Administrative Region of China
[d] Shanghai Synchrotron Radiation Facility, Shanghai Advanced Research Institute, Chinese Academy of Sciences, Shanghai, 201204, PR China
[e] Department of Applied Biology and Chemical Technology, Faculty of Science, The Hong Kong Polytechnic University, Kowloon, 99077, Hong Kong Special Administrative Region of China

ARTICLE INFO

Keywords:
Polymer brush
Poly (glycidyl methacrylate)
Surface modification
Protein immobilization
Bioactivity

ABSTRACT

Preservation of growth factor sensitivity and bioactivity (e.g., bone morphogenetic protein-2 (BMP-2)) post-immobilization to tissue engineering scaffolds remains a great challenge. Here, we develop a stable and soft surface modification strategy to address this issue. BMP-2 (a model growth factor) is covalently immobilized onto homogeneous poly (glycidyl methacrylate) (PGMA) polymer brushes which are grafted onto substrate surfaces (Au, quartz glass, silica wafer, or common biomaterials) via surface-initiated atom transfer radical polymerization. This surface modification method multiplies the functionalized interfacial area; it is simple, fast, gentle, and has little effect on the loaded protein owing to the cilia motility. The immobilized BMP-2 (i-BMP-2) on the surface of homogeneous PGMA polymer brushes exhibits excellent bioactivity (~87% bioactivity of free BMP-2 *in vitro* and 20%–50% higher than scaffolds with free BMP-2 *in vivo*), with conformation and secondary structure well-preserved after covalent immobilization and ethanol sterilization. Moreover, the osteogenic activity of i-BMP-2 on the nanoline pattern (PGMA-poly (N-isopropylacrylamide)) shows ~110% bioactivity of free BMP-2. This is superior compared to conventional protein covalent immobilization strategies in terms of both bioactivity preservation and therapeutic efficacy. PGMA polymer brushes can be used to modify surfaces of different tissue-engineered scaffolds, which facilitates *in situ* immobilization of growth factors, and accelerates repair of a wide range of tissue types.

1. Introduction

Growth factors (GFs), a type of secreted proteins produced by animal cells, regulate a series of cellular behaviors including survival, migration, proliferation and differentiation [1]. For example, bone morphogenic protein-2 (BMP-2), one of the few Food and Drug Administration (FDA) approved GFs, plays a crucial role in inducing new bone formation in ectopic sites and bone defects [2–6]; it has been incorporated into various scaffolds as bone regeneration therapeutics [7–12]. To equip the scaffolds with local and controlled GF delivery, many researches focused on modifying scaffold surfaces with the heparin-based direct binding approach as it resembled the natural interaction between the extracellular matrix (ECM) and the proteins [13–15]. These approaches, however, suffer from low protein binding efficiency and rapid protein release due to the weak electrostatic interactions. Covalent immobilization of GFs has thus been developed to eliminate the initial burst release and to

Peer review under responsibility of KeAi Communications Co., Ltd.
* Corresponding author.
** Corresponding author.
*** Corresponding author. Laboratory for Advanced Interfacial Materials and Devices, School of Fashion and Textiles, The Hong Kong Polytechnic University, Kowloon, 99077, Hong Kong Special Administrative Region of China.
E-mail addresses: liucs@ecust.edu.cn (C. Liu), xin.zhao@polyu.edu.hk (X. Zhao), tczzheng@polyu.edu.hk (Z. Zheng).

https://doi.org/10.1016/j.bioactmat.2022.12.029
Received 30 August 2022; Received in revised form 29 December 2022; Accepted 29 December 2022

improve the stability and endurance of proteins transport to cells or tissues [16–18]. Delivery of covalently immobilized GFs would have a controllable and sustainable influence on cell behaviors, with many advantages over soluble or slowly released proteins [19,20]. Unfortunately, the rigid covalent bonding limits the orientation of biomolecules, which may obscure essential surface reactive sites and hinder their bioactivity [21,22]. The interference between charged groups within larger molecules such as GFs also limits the amount of directly immobilized molecules on the material surface. Hence, researchers have investigated methods of increasing the reactive surface on a tissue engineering scaffold, of which polymer brush grafting received notable attention owing to its ability to anchor brushes of controllable length and grafting density onto most material surfaces. Its flexibility to work with a diverse range of polymer materials allows for excellent modulation of basic surface properties of the bulk tissue scaffolds, while also enabling specific reaction cues on the polymer brushes in terms of both niche functional groups and side chains, creating a near infinite possibility of combinations in coating medical devices and scaffolds.

In this work, we develop a surface-initiated atom transfer radical polymerization approach (SI-ATRP) to tailor the functionality of surface of various biomaterials with covalently tethered polymer brushes for immobilization of GFs. The densely packed polymer brush surface acts as motile artificial cilia, capable of loading GFs, and moves under fluid movements. We use BMP-2 as a model GF due to its high bioactivity in regulating cell behaviors, high abundance of active groups for surface modification process and high relevance in clinical applications. Through functionalization of various biomaterial surfaces (Au, quartz glass, silica wafer, polycaprolactone, poly (methyl methacrylate) or poly glycerol sebacate/β-tricalcium phosphate (TCP)) with well-defined polymer brushes (i.e., poly (glycidyl methacrylate) (PGMA)-poly (N-isopropylacrylamide) (PNIPAm)) of controlled length and density, successful immobilization of sensitive BMP-2 with no detrimental effect on its bioactivity has been achieved, both *in vitro* and *in vivo*. We envision our covalent immobilization strategy will have great potential in surface functionalization and modification of many tissue engineering scaffolds by controlling the local biomacromolecule conjugation.

2. Materials and methods

2.1. Materials

The chemical reagents involved in our experiments are listed as follows: glycidyl methacrylate (GMA, Mw 142.2) was purchased from J&K company. N-isopropylacrylamide (NIPAm, Mw, 113.2), copper(I) bromide (CuBr, Mw 143.5), 2,2′-bipyridyl (bPy, Mw 156.2), ω-mercaptoundecyl bromoisobutyrate (MUDBr), sodium azide (NaN_3, Mw 65.01), N,N-dimethyl formamide (DMF, Mw 73.1), L-ascorbic acid (VC, Mw 176.1) and gelatin were all purchased from Sigma-Aldrich. Methanol (Mw 32.05) and dichloromethane (Mw 84.93) were purchased from Duksan Ltd. Toluene (Mw 92.1), acetone (Mw 58.1), ethanol (Mw 46.1) and 2-propanol (Mw 60.1) were all purchased from VWR-BDH Co. Ltd. Phalloidin-Rhodamine, DAPI and MTS (3-(4,5-dimethylthiazol-2-yl)-5-(3-carboxymethoxyphenyl)-2-(4-sulfophenyl)-2H-tetrazolium) were purchased from Sigma-Aldrich. Alkaline phosphatase (ALP) Kit and Bicinchoninic Acid (BCA) Kit were from Beyotime Bio Company, while the BMP-2 ELISA kit (QuantiCyto®) was purchased from Neobioscience Co. Ltd. All cell-culture related reagents were purchased from Gibco Co. Ltd.

2.2. Fabrication of PGMA polymer brush-coated Au substrate

PGMA polymer brush-modified Au substrate was prepared by growing PGMA brushes on the MUDBr self-assembled monolayers (SAM) via SI-ATRP. Firstly, the MUDBr-Au substrate was soaked with prepared reaction solution in a 100 mL centrifuge tube. The reaction solution was composed of methanol (9.6 g), GMA (15.6 g), deionized water (3.0 g), bPy (0.42 g), CuBr 0.156 g) and ascorbic acid (0.6 g). The reaction temperature and polymerization time were 40 °C and 150 min respectively. The prepared substrate was then washed with deionized water, methanol, acetone and toluene, dried with N_2 stream at 60 °C and then terminated with NaN_3 (200 mg of NaN_3 dissolved in 30 mL of DMF). At last, the substrate was dried and placed in a vacuum desiccator.

2.3. Synthesis of PGMA-BMP-2 substrate

The prepared PGMA substrate was sterilized with 70% alcohol and washed three times with phosphate buffer saline (PBS). Then the substrate was immersed in BMP-2 solution at 37 °C for 4 h. In our experiment, the initial concentration of BMP-2 solution is 2 μg/mL and the volume of loading solution is 2 mL. The PGMA-BMP-2 substrate was vortex washed with PBS 4 times for 5 min each. Then, the washing liquid was collected, and the concentration of the BMP-2 solution before and after the loading was detected with the BMP-2 ELISA kit, and the amount of BMP-2 immobilized onto the PGMA surface was calculated. The density of BMP-2 on the polymer brush is calculated as the amount of BMP-2 on the polymer brush divided by the surface area of the polymer brush.

2.4. Preparation of nanoline patterned PGMA-PNIPAm binary polymer brushes

According to the experimental protocol of our previous work [23–26], we first synthesized thin PNIPAm polymer brushes. We then fabricated the PNIPAm polymer brushes with SI-ATRP. Briefly, the initiator of MUDBr was modified onto the surface of Au substrate and placed into the prepared reaction solution in a 50 mL centrifuge tube. The reaction solution was made of NIPAm (1.5 g), deionized water (15 g), methanol (12 g), PMDETA (165 mL), CuBr (0.048 g) and ascorbic acid (0.4 g). The reaction temperature and polymerization time were 40 °C and 5 min respectively. The prepared substrate was then washed with deionized water, methanol, acetone and toluene, and then dried with N_2 stream at 60 °C and terminated by NaN_3 (200 mg of NaN_3 dissolved in 30 mL of DMF). Then with our large-area dip-pen nanodisplacement lithography (DNL) patterning method [23–26], we inked the 55,000-tip cantilever array with MUDBr by immersing it in MUDBr solution for 15 s and drying in air. With atomic force microscope (AFM) instrument and XEP software, the PNIPAm brushes on the gold substrate were scraped by the MUDBr-inked tip array and the MUDBr small molecules were self-assembled onto the bare gold surface. After that, the MUDBr patterned PNIPAm brush modified substrate was placed within PGMA reaction solution (same as section 2.2) in a 50 mL centrifuge tube. Then the resulting PGMA-PNIPAm binary polymer brushes were washed with deionized water (3 times), methanol (3 times), acetone and toluene (twice), and then dried *via* N_2 stream.

2.5. Fabrication of biomaterials modified with PGMA polymer brushes

We have selected three common polymer tissue engineering materials – polycaprolactone (PCL), poly methyl methacrylate (PMMA) and poly glycerol sebacate/β-TCP (PGS/β-TCP) as substrate and attached the PGMA polymer brushes onto their surfaces. Take the preparation of PCL-g-PGMA film for example, we first prepared PCL film with spin coating method. The PCL thin film was then treated with plasma to generate the hydrolyzed PCL-OH film. Immediately, the PCL-OH film surface was immobilized with ATRP initiator (3-(trichlorosilyl) propyl 2-bromo-2-methylpropanoate) *via* the reaction of the hydroxyl group with trichlorosilane group. With vapor deposition, the bromine group was modified onto the surface of PCL film. PGMA polymer brushes was then grafted onto the surface with SI-ATRP. Prior to drying under decreased pressure, the PCL-g-PGMA surface was completely washed with water and methanol after the reaction to guarantee full removal of the

significantly adsorbed reactants. Then BMP-2 was immobilized onto the surface as mentioned above. At the same time, we prepared the PMMA-g-PGMA to immobilize BMP-2. We additionally 3D printed PGS/β-TCP scaffolds (common composite bone repair material) with 30% PGS and 70% β-TCP as ink through a precision 3D printing system developed by Regenovo Bio-Architect WS (Regenovo, China) according to literature [27,28]. After that, we prepared PGS/β-TCP-g-PGMA to immobilize BMP-2.

2.6. Characterization of polymer materials modified with PGMA polymer brushes

AFM images were obtained by the XE-100 AFM system manufactured by Park Systems in South Korea and measured in non-contact mode at room temperature. The high resolution X-ray photoelectron spectroscopy (XPS) experiments were conducted by PHI–5000C ESCA system upgraded with RBD (PerkinElmer, USA) with Al Kα radiation to characterize the PGMA and PGMA-BMP-2 substrate. Raman spectra were measured by an RM 1000 Raman spectrometer (Renishaw Plc., UK) with a 532 nm laser. Data analysis was implemented using XPSPEAK41 software. Attenuated total reflection Fourier transfer infrared spectroscopy (ATR-FTIR) was carried out using a PerkinElmer Spectrum 100 FI-TR spectrometer (PerkinElmer Inc., US).

2.7. Cell culture

C2C12 cells were purchased from American Type Culture Collection (ATCC). C2C12 cells were cultured in 60 mm dishes with DMEM (Gibco, NY) containing 10% fetal calf serum (Gibco, NY), double antibiotics at 37 °C in a CO_2 incubator. The cell density was calculated before experiment and then the cells were cultured at the desired density in later experiments.

2.8. Biocompatibility of PGMA polymer brushes

Biocompatibility of PGMA polymer brushes and the materials modified with PGMA polymer brushes was evaluated with MTS assay. C2C12 cells were plated with substrates into 12-well plates at a density of 2.0×10^4 cells per well in 2 mL culture medium, and cultured for 1, 2 and 3 days. The MTS assay was determined using a standard procedure after each culture duration respectively. A standard medium without samples was used as a positive control for cell viability. All samples have three parallel samples. Cell viability results were expressed as mean ± SD as percentage of the control group (100% viability). The biocompatibility of PGMA polymer brushes and PGMA-BMP-2 was also observed after 3 days by staining the nucleus with DAPI. The cell morphology was observed with a Leica TCS SPE confocal microscope.

2.9. Measurement of ALP activity

To measure the ALP activity, C2C12 cells were seeded into 12-well plates with substrates or blank plates at 5×10^4 cells per well in DMEM. The culture medium was changed to 2 mL DMEM with various doses of BMP-2 solution after the cells were adhered for 12 h. The plates with substrates were replaced with 2 mL DMEM. The culture medium was aspirated after 3 days. The wells were then filled with about 300 mL of 1% NP40 (nonidet P-40), and then incubated for 60 min at room temperature. 50 mL cell lysate and 50 mL 2 mg/mL PNPPNa (p-nitrophenylphosphate, Beyotime, China) substrate solutions were added into a 96-well plate. The color reaction was quenched by 100 mL of 0.1 M NaOH after 15 min of incubation at 37 °C. The ALP value was calculated using a microplate reader (LEDETECT 96) at a wavelength of 405 nm. ALP activity was measured in our study as 405 nm O.D. value per min per mg of total protein. The ALP activity was also histochemically detected using 5-Bromo-4-Chloro-3-Indolyl Phosphate/Nitroblue tetrazolium chloride (BCIP/NBT) ALP color development kit (Beyotime, China) after 3 days of culture.

2.10. Conformation and secondary structure of immobilized BMP-2 (i-BMP-2)

Circular dichroism (CD) spectroscopy is one of the most important technology for the measurement of proteins' conformation and secondary structure. In our research, we were able to identify the BMP-2 conformation that was immobilized on the surface of PGMA. PGMA polymer brushes were prepared on the surface of the quartz glass using the method as before, followed by immobilization of BMP-2 and further detection of the conformation of BMP-2 using CD spectroscopy (J-1500, JASCO, Japan). The analysis of the free and released BMP-2 took place at 25 °C in a 1.0 mm path length quartz cell with a scan rate of 100 nm/min and a time constant of 0.25 s. The Far-UV CD spectrum (190–260 nm) was measured. Free BMP-2 used was 2 μg/mL and 5 scans were accumulated.

2.11. Real-time reverse transcription polymerase chain reaction (Real-time RT-PCR) assay

C2C12 cells were cultured with PGMA-BMP-2 substrates or blank plates at 8×10^4 cells per well in DMEM. After cell adhesion, the culture medium was changed to fresh DMEM or DMEM containing a specific concentration of BMP-2. After 1, 3 and 5 days' incubation, the total cellular RNA of C2C12 cells was extracted according to the standard procedure. The first-stranded cDNA was synthesized using PrimeScript RT Reagent Kit. And then, it was diluted 10-fold in deionized water. Real-time RT-PCR was performed in a 10 μL solution containing 4 μL of the diluted cDNA, 5 μL of 1 × SYBR Premix Ex Taq, 0.4 μL of 0.2 mM of each primer (please see Table s4 for details of primer used), and 0.2 μL of ROX Reference Dye (50 ×). The conditions of real-time RT-PCR were as follows: 95 °C for 30 s, followed by 40 cycles at 95 °C for 5 s and 60 °C for 34 s. We have researched four cell differentiation markers, runt-related transcription factor 2 (Runx2), collagen I (Col I), ALP and osteocalcin (OCN) by a Bio-Rad real-time PCR system (Bio-Rad, US).

2.12. In vivo cranial defect model and scaffold implantation

The rat cranial critical-sized defect model was used to study the *in vivo* osteogenic effects of the polymer brush-immobilized BMP-2. A total of 24 adult male SD rats with an average weight of ~220 g was purchased from the National Tissue Engineering Center (Shanghai, China) with the approval of the Animal Research Committee of the Sixth People's Hospital, Shanghai Jiao Tong University School of Medicine (License number: SCXK (Hu)2021-0004). Four groups of these rats were randomly assigned. Briefly, after anesthetization, the skin and cranial periosteum of rats were detached, and under sterile saline washing, two symmetrical 5 mm diameter cranial defects were produced with a bone trephine bur (RWD, China). The defects were then filled by 4 kinds of scaffolds: PGS/β-TCP scaffolds, PGS/β-TCP-PGMA scaffolds, PGS/β-TCP-BMP-2 scaffolds and PGS/β-TCP-PGMA-BMP-2 scaffolds (5 mm diameter and 1.5 mm height). BMP-2 used in all animal experiments was 2.5 μg/per sample. After surgery, absorbable sutures were used to stitch the incision layer by layer. The rats were euthanized after 6 and 12 weeks, and samples were collected for further μCT and histology analysis.

2.13. Synchrotron radiation-based μCT analyses

Synchrotron radiation-based CT (SRCT) measurements were carried out on beamline BL13W of the SSRF (Shanghai Synchrotron Radiation Facility, Shanghai, China) using a monochromatic beam with an energy of 40 KV in order to investigate the *in vivo* bioactivity of the BMP-2 and assess the healing process of bone abnormalities. The sample-to-detector distance was 18 cm with a scanning accuracy of 9 μm. In our current

research, images were recorded using a 4000 × 2500 CCD detector with a pixel size set to 6 μm. Finally, the images were re-digitized in an 8-bit data format and put through further 3D processing. The software of VG Studio MAX 2.0 (Volume Graphics, Germany) was used for visualization of the tomographic data. Bone radio morphometric analysis was carried out by using MicroView 2.2 ABAA software (GE Health Systems, USA). Following 3D reconstruction, the bone volume/total volume (BV/TV) and trabecular thickness (Tb.Th) were automatically calculated.

2.14. Histological staining

After SR-CT analysis, samples underwent a 6-week decalcification process in 12.5% EDTA solution. After that, samples were dehydrated with graded ethanol and embedded in paraffin, and the 4 μm thickness sections were sliced and stained for Masson's trichrome (MT) and immunofluorescence analysis. For immunofluorescence staining, proteins labeled with CD31 (1:50, Abcam, UK) and OCN (1:50, Abcam, UK) antibodies were stained brown to identify blood vessels and osteogenesis. The Leukocyte Acid Phosphatase Assay (Sigma-Aldrich, USA) was used in accordance with the manufacturer's instructions to perform tartrate-resistant acid phosphatase (TRAP) staining to assess the bone-resorbing activity. The staining slides were all photographed using a digital camera and a light microscope (Axio Scope A1, Germany) (SPOT Flex, USA).

2.15. Statistical analysis

Data were expressed as the mean ± standard deviation (SD). In our experiments, statistical analysis was carried out with one-way analysis of variance (ANOVA). A value of $p < 0.05$ was regarded as statistical significance.

3. Results and discussion

3.1. Synthesis and characterization of PGMA brushes

We first introduced SI-ATRP initiator ω-mercaptoundecyl bromoisobutyrate (MUDBr) to Au surface in preparation for polymerization (Fig. 1a). Then well-defined PGMA brushes were propagated via SI-ATRP from the Au–Br surface. Here, a ring-opening reaction was performed to directly couple the dense functional epoxide groups on the grafted PGMA brushes to the amine groups of BMP-2. According to AFM results (Fig. 1b–d), it can be seen that the surface roughness of Au, Au-PGMA and Au-PGMA-BMP-2 are 0.34 nm, 3.24 nm and 3.7 nm, respectively. The results proved that the surface roughness of the material improved with the bonding of the PGMA polymer brush, while the roughness of PGMA is slightly improved after immobilization with BMP-2. It also indirectly demonstrated the formation of polymer brush and further immobilization of BMP-2. The polymer brush also has reactive epoxy groups on the side chains, so the growth factor BMP-2 can be immobilized on the surface and/or inside the polymer brush. Our experimental results also confirm that the thickness of the polymer brush increased by 15–20 nm after the immobilization of BMP-2. As the molecular volume of BMP-2 is 7 nm * 3.5 nm * 3.5 nm, our results indicated that the immobilization of BMP-2 on the polymer brush is a multilayer adsorption. Raman spectroscopy was used to analyze the chemical bond composition on the designed substrates to validate the attachment of BMP-2 to PGMA-coated Au substrates (Fig. 1e). The immobilization of BMP-2 protein changed the chemical bond composition of the PGMA surface, as seen by the Raman spectra. When the laser wavelength was set as 532 nm, a sharp peak at 517 cm^{-1} appeared which corresponded to the characteristic peak for disulfide bond (S═S) of BMP-2. This result proved that BMP-2 existed on the surface of PGMA brushes. Additionally, XPS spectra showed that BMP-2 immobilization changed the chemical composition of the PGMA surface. A prominent nitrogen (N1s) atomic elemental peak was seen on the BMP-2-immobilized PGMA surface at 400 eV. (Fig. 1f). The XPS analysis used

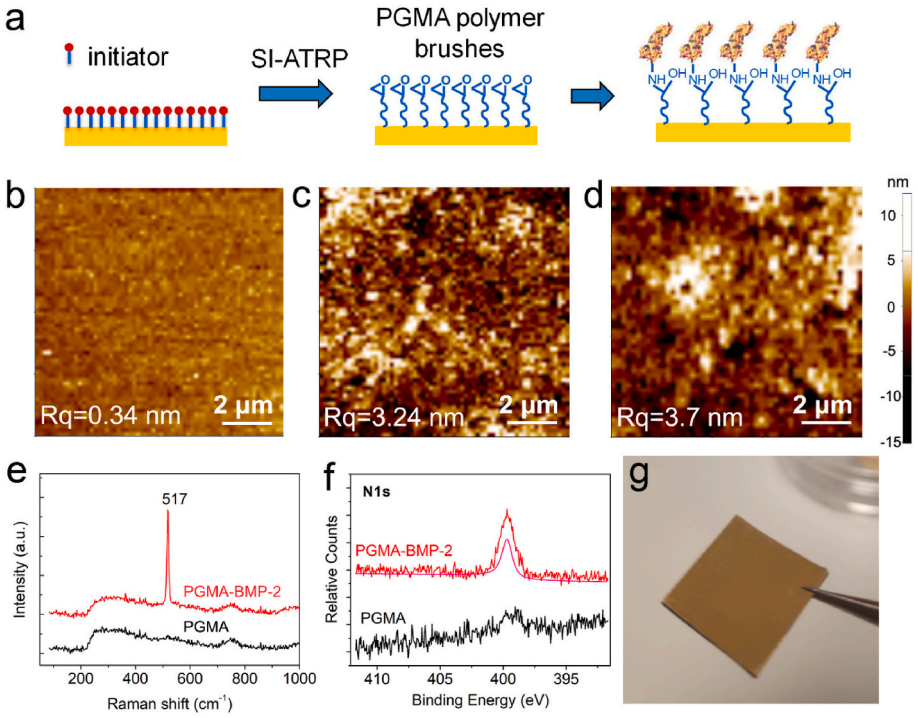

Fig. 1. Immobilization of BMP-2 on the surface of PGMA and characterization of the PGMA and PGMA-BMP-2. (a) Scheme of preparation of PGMA-BMP-2; (b–d) AFM images of Au, Au-PGMA and Au-PGMA-BMP-2 surfaces; (e) Raman spectra of PGMA brushes and PGMA-BMP-2; (f) XPS spectra of N 1s of PGMA polymer brushes and PGMA-BMP-2; (g) Digital images of prepared PGMA-BMP-2 on Au substrate.

to quantify the atomic chemical composition showed that the N content of the surfaces of PGMA and PGMA-BMP-2 were 0% and 13.91%, respectively. After PGMA was prepared onto the surface of Au substrate with ATRP, nitrogen was not detected at all (0%) on the surface. This indicated the thorough coating of PGMA onto the Au substrate. However, the quantity of nitrogen dramatically increased (13.91%) after BMP-2's immobilization onto the PGMA surface, indicating its successful coupling. We also determined the ratio of the substrate surface's atomic chemical composition (O/C ratio and N/C radio) before and after functionalization (Table s1). Specifically, the ratio of N/C of PGMA-BMP-2 surface (N/C = 0.207) approached the theoretical value of BMP-2 itself (N/C = 0.24). These results suggested that the immobilization of BMP-2 onto the PGMA surface through a simple ring-opening conjugation was successful.

C2C12 cells are commonly used model cells to research the bioactivity of BMP-2 [29–31]. We selected C2C12 cells because the expression of ALP in C2C12 cells was markedly higher than that in BMSCs under the same concentration of BMP-2, which was very beneficial to investigate the activity of BMP-2 at low concentration. The biocompatibility of PGMA polymer brush was then measured using C2C12 cells with the MTS (3-(4, 5-dimethylthiazol-2-yl)-5-(3-carboxymethoxyphenyl)-2-(4-sulfophenyl)-2H-tetrazolium) assay, a widely used method to measure the mitochondria activity to quantify the cell growth/viability (Fig. 2a). According to the MTS results, the cell viability of PGMA polymer brush and BMP-2-immobilized PGMA (PGMA-BMP-2) were as good as the controlled samples (polystyrene cell culture plate) after 3 days of culture. MTS results of PGMA-BMP-2 on different substrates (Au, quartz glass, silica wafter) showed comparable results as the control polystyrene plates (Fig. 2b). These results indicated that the PGMA polymer brush was biocompatible. We used Au, quartz glass, and silica wafter as substrate materials as they are frequently modified by BMP-2 for different medical purposes (e.g., to research BMP-mediated signaling and cell migration, GF delivery for bone regeneration) [32,33]. Furthermore, when the PGMA polymer brush was immobilized with BMP-2, the C2C12 cells were induced to osteogenic differentiation and resulted in a certain inhibitory effect on its proliferation. The cell density counted *via* DAPI staining (Fig. s1) on the PGMA polymer brushes and PGMA-BMP-2 were all as good as the controlled polystyrene plates. These results correspond to the results of MTS measurement and further confirmed that the PGMA polymer brush was biocompatible.

In a parallel study, C2C12 cells were cultured on PGMA polymer brushes and PGMA-BMP-2 to evaluate the effect of polymer surfaces with immobilized protein on cell adhesion. The cytoskeleton of cells was stained red by phalloidin-Rhodamine and the nuclei were stained blue by DAPI (Fig. 2c). After culturing for 24 h, the C2C12 cells cultured on PGMA-BMP-2 had an osteoblast-like polygonal morphology, while the cells on PGMA polymer brush maintained a spindle shape. The size of the spindles on PGMA polymer brush was much smaller. The different morphology was mainly resulted from the differentiation of C2C12 cells when cultured with PGMA-BMP-2. Previous results [34] demonstrated that bioactive BMP-2 has the ability to induce the differentiation of C2C12 into osteoblasts. Our results further proved that the i-BMP-2 maintained the bioactivity and physiological function to facilitate the osteogenic differentiation of C2C12 cells.

3.2. *Bioactivity of i-BMP-2*

To determine whether the i-BMP-2 has osteogenic activity, ALP activity of C2C12 cells was measured after a 3-day incubation period. Our results manifested that the i-BMP-2 on the PGMA polymer brush showed very good osteogenic bioactivity (Fig. 3a–b). Through quantitative ALP activity assay and qualitative ALP staining experiment, we pleasantly found that the i-BMP-2 had up to 87% activity of free BMP in solution. However, the bioactivity of surface immobilization of BMP-2 via a self-assembled monolayer formation was about 60% compared to BMP-2 in

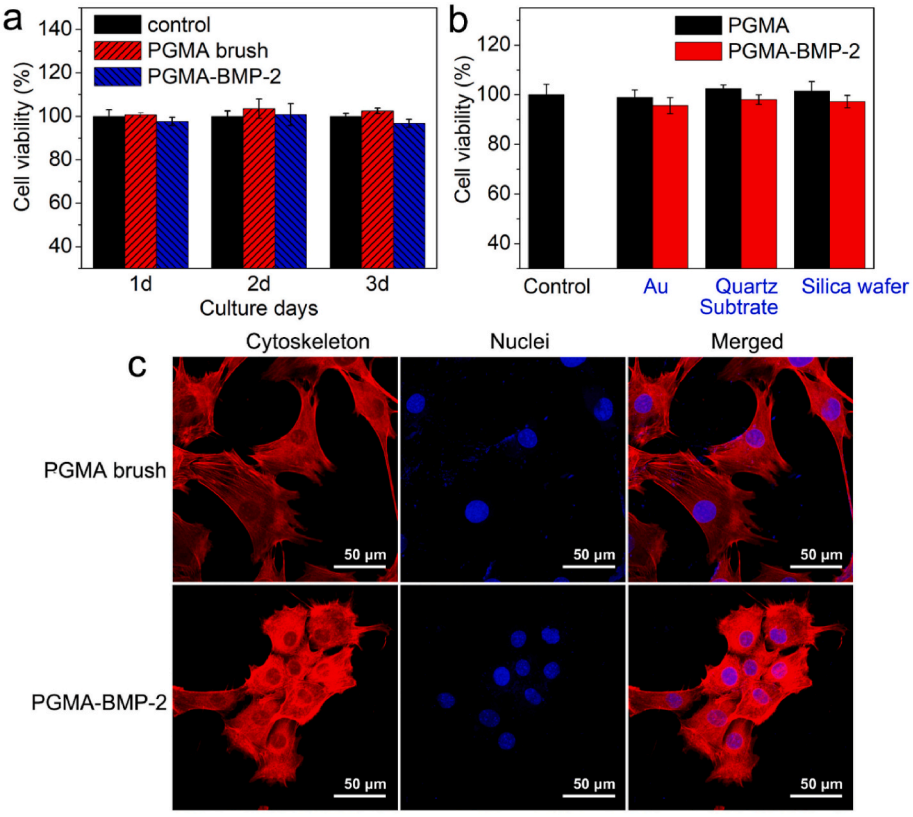

Fig. 2. Biocompatibility of PGMA polymer brushes and PGMA-BMP-2. (a) MTS results of PGMA polymer brushes and PGMA-BMP-2; (b) MTS results of PGMA-BMP-2 on different substrates; (c) Cell morphology of C2C12 cells on the surface of PGMA brushes and PGMA-BMP-2.

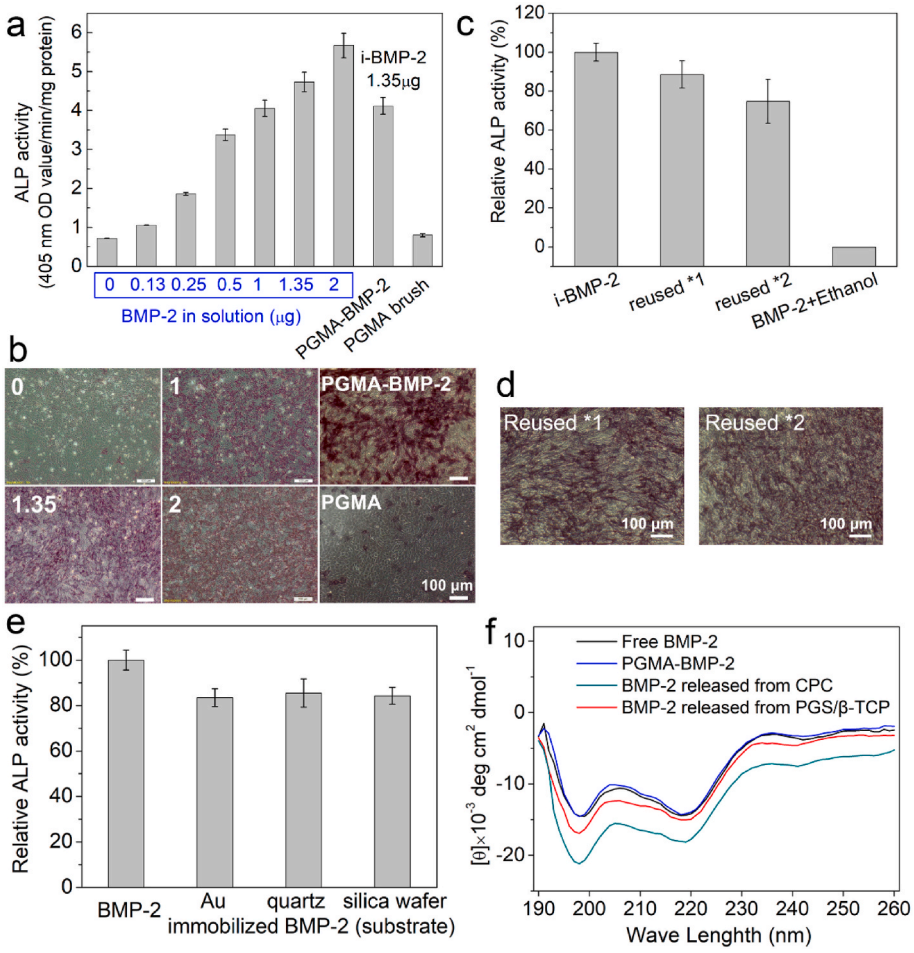

Fig. 3. Bioactivity of PGMA-BMP-2 with C2C12 cells. (a) ALP activity of PGMA-BMP-2 (i-BMP-2) and BMP-2 in solution; (b) ALP staining of PGMA-BMP-2; (c) Relative ALP activity of reused PGMA-BMP-2; (d) ALP staining of reused PGMA-BMP-2; (e) Relative ALP activity of PGMA-BMP-2 on different substrates; (f) Circular dichroism measurement of BMP-2 in solution, the i-BMP-2 (PGMA-BMP-2), BMP-2 released from PGS/β-TCP and CPC. The amount of BMP-2 immobilized on the PGMA polymer brushes is 1.35 μg.

solution [35]. BMP's biological activity was nearly entirely lost when it was bound to the silica surface by stable secondary amine bonds, and only partially regained when the protein was freed by hydrolysis of the surface siloxane and ester bonds [36]. We also found that the PGMA-BMP-2 could maintain its bioactivity after sterilization treatment with cell lysis and alcohol (Fig. 3c–d). This is advantageous to popularize our technique as it indicates that the protein conformation and secondary structure are well-reserved after covalent immobilization and ethanol sterilization. In addition, the ALP activity of C2C12 cultured with BMP-2 immobilized on different substrates was between 82% and 88%. It is worth noticing that the PGMA-BMP-2 boasted good ALP activity, even after reuse (treated with cell lysis buffer and alcohol) and on different substrates (Fig. 3e).

Protein-ligand binding reactions often mediate the bioactivity of proteins via alteration of the secondary structure. To prove that the protein conformation and the secondary structure of BMP-2 can be maintained after our surface modification process, BMP-2 was immobilized onto the surface of quartz glass. The secondary structure of BMP-2 immobilized on PGMA surface was determined by far-UV CD spectroscopy (Fig. 3f). The secondary structure content of BMP-2 in solution, immobilized BMP-2 (i-BMP-2), BMP-2 released from calcium phosphate cement (CPC), and BMP-2 released from PGS/β-TCP were summarized in Table s2. The percentages of α-helix, β-sheet and β-turn, and random coil for free BMP-2 in deionized water were 16.3%, 15.67%, 15.46% and 52.57%, respectively. α-helix of BMP-2 increased after immobilization with PGMA while that of BMP-2 released from CPC and PGS/β-TCP decreased. The transforms of the folding structure of i-BMP-2, BMP-2 released from PGS/β-TCP and from CPC were 2.2%, 7.66% and 12.3%, respectively. As anticipated, the CD spectra manifested that i-BMP-2 could maintain the most helix protein structure and lead to the least change of the folding structure. These results confirmed that immobilization of BMP-2 with PGMA could maintain the secondary structure and well preserve the bioactivity of BMP-2.

Whether proteins change structurally is significantly affected by the nature of the adsorbed proteins and the chemistry, stiffness, size, and curvature of the solid surfaces [37–39]. Among these factors, the stiffness of PGMA polymer brushes is closely related to its thickness (molecular chain length). Therefore, we prepared a range of PGMA polymer brushes with different chain length by adjusting the monomer concentration and reaction time of ATRP. According to the thickness of brushes, for example, for PGMA polymer brushes with a thickness of 5 nm, we named it as PGMA-5. We have prepared in total 6 different thicknesses of PGMA, including PGMA-5, PGMA-12, PGMA-27, PGMA-41, PGMA-79 and PGMA-100. By detecting the concentration of BMP-2 solution before and after loading, we could calculate the amount of BMP-2 immobilized on the PGMA polymer brush. The immobilization efficiency of BMP-2 on uniform PGMA polymer brush surface was 1.7 μg/cm^2 (Fig. s2). We loaded the same amount of BMP-2 using the same method as before, and then co-cultured with C2C12 cells to detect the corresponding ALP activity. We found that the ALP activity of PGMA-BMP-2 was about 75%–90% of free BMP-2 in solution, and the difference between different thicknesses of PGMA-X-BMP-2 (X is thickness) is not obvious (Fig. s3). We further selected PGMA-5-BMP-2, PGMA-41-BMP-2 and PGMA-100-BMP-2 to detect their secondary structural change using CD. We found that there was no obvious difference between these three samples (Fig. s4). The free BMP-2 in PBS showed two negative peaks at 208 nm and 220 nm, which correspond to the BMP-2-helix, as well as a strong positive peak at 195 nm. After

immobilization with PGMA, α-helix of BMP-2 increased in all the three samples. The change of the folding structure of PGMA-5-BMP-2, PGMA-41-BMP-2 and PGMA-100-BMP-2 was 2.48%, 2.6% and 2.2%, respectively (Table s3). From the results, we can see that different thickness of PGMA-X-BMP-2 has little effect on the secondary conformation of the protein, which makes the α-helix structure increase slightly, and the total change of the folded structure is between 2.2% and 2.6%. Consequently, we can conclude that the thickness of PGMA brush does not have significant effect on the structure of i-BMP-2. This may explain why the difference in ALP activity of PGMA-X-BMP-2 is not obvious.

3.3. Evaluation of the selective covalent binding of BMP-2 with PGMA

To detect the selective covalent binding of BMP-2 with PGMA and further confirm the biological activity of i-BMP-2, we prepared PGMA@PNIPAm nano-micro binary systems with spacing of 2 μm (for enhanced cell alignment) using a typical DNL fabrication method (Fig. 4a–b). According to our previous work [23], gelatin-PGMA@PNIPAm binary polymer brushes fabricated by the DNL technique could provide ideal ECM-like structure for cell growth and orientation. We co-cultured C2C12 cells with the nanoline pattern with spacings of 2 μm, 4 μm, 6.7 μm and 20 μm, respectively (Fig. S5). We found that the orientation of the cells was the most obvious when the spacing of the nanoline was 2 μm. We thus used samples with spacing of 2 μm in this research. The loading of BMP-2 and gelatin for these patterns are 6.8 and 2713 μg/cm^2, respectively. The role of the gelatin here is to promote the adhesion and orientation of the cells. The loading of BMP-2 on patterns is markedly higher than that on the uniform PGMA polymer brushes. This may be attributed to that when the polymer brush is loaded with protein in the solution, the molecular chain of PGMA is in an expanded state, so BMP-2 not only reacts with the epoxy group on the surface of the polymer, but also with the epoxy group in the middle of the molecular chain. Furthermore, with the same amount of BMP-2 in solution as positive control, the ALP activity of BMP-2 immobilized on the nanopatterns is obviously higher than that on the homogeneous PGMA surface (Fig. 4c). After 24 h incubation, it was found that the pseudopods of C2C12 cells were extended with the PGMA nanoline with 2 μm spacing (Fig. 4d). We thus believe that the 2 μm spacing is favorable for cell orientation and it has a certain enhancement for the cell differentiation promoted by BMP-2.

3.4. The versatility of surface modification strategy with PGMA brushes

Lastly, to demonstrate the versatility of our surface modification strategy, we further modified PCL, PMMA and PGS/β-TCP surfaces with PGMA brushes using SI-ATRP (Fig. s6 & Fig. s7). The water contact angle of PCL film was about 84°. After treatment with plasma, the water contact angle reduced to 51°, which indicated that the hydroxyl groups generated on the surface increasing the hydrophilicity of the surface. When the surface of film was immobilized with ATRP initiator, the water contact angle increased to 67°, which is consistent with that the Br-containing ATRP initiator has certain hydrophobicity. At last, the water contact angle of PCL-g-PGMA film was about 81°, which was also consistent with the result of the surface hydrophobicity of PGMA. Similarly, the water contact angle of PMMA film was about 63°. The water contact angle of PMMA-OH, PMMA-Br, and PMMA-g-PGMA film was 51°, 67°, and 81°, respectively (Fig. s7). These findings showed that the functionalization of PGMA polymer brushes onto the surface of PMMA and subsequent immobilization with BMP-2 were effective. The immobilization of BMP-2 onto the surface of PCL-g-PGMA and PMMA-g-PGMA can also maintain the protein conformation and well preserve the bioactivity of BMP-2 (Fig. s8). From the water contact angle results (Fig. s9), we can find that the water contact angle of PGS/β-TCP materials is about 76°. After treatment with plasma, the water contact angle reduced to 38°. At last, when the PGMA polymer brushes has been modified on the surface, the water contact angle of the PGS/β-TCP-g-PGMA film became about 84°. From the ATR-FTIR of PGS/β-TCP-g-PGMA (Fig. s11), we can find that a peak at 909 cm^{-1} appeared which corresponded to the characteristic peak of the epoxidation group of PGMA polymer brushes. These above results demonstrate that our surface modification strategy can be applied to various tissue engineering materials.

3.5. Effect of i-BMP-2 on the mRNA expression of osteoblast markers

The gene expression of related osteoblast markers was measured via real-time RT-PCR analysis (Fig. 5). ALP and Col-I are early markers of

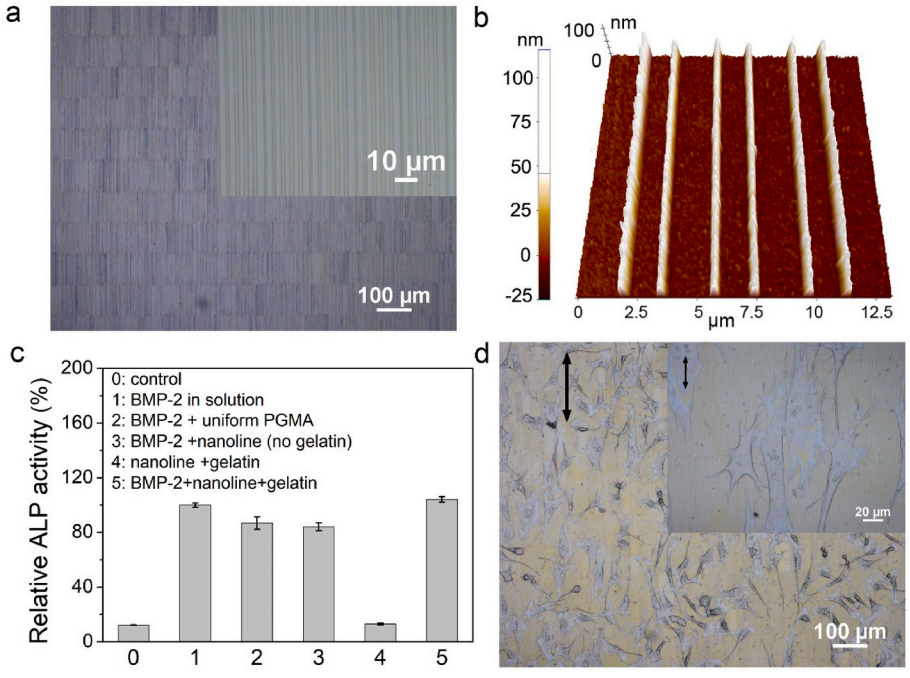

Fig. 4. Evaluation of the selective covalent binding of BMP-2 with PGMA@PNIPAm nano-micro binary systems. Optical images (a) and AFM topographic images (b) of BMP-2/gelatin-PGMA@PNIPAm nanoline sample. (c) Relative ALP activity of BMP-2 immobilized on uniform PGMA, BMP-2 on nanolines with no gelatin, gelatin-PGMA@PNIPAm nanoline pattern and BMP-2/gelatin-PGMA@PNIPAm. (d) Optical photographs of C2C12 cells incubated on the BMP-2/gelatin-PGMA@PNIPAm substrate for 24 h.

osteoblastic differentiation while OCN is a late osteogenic differentiation marker. Meanwhile, a bone-specific transcription factor called Runx2 guides pluripotent mesenchymal cells toward their osteoblast lineage. After co-culturing C2C12 cells with PGMA-BMP-2 and soluble BMP-2, it was found that the ALP mRNA expression of both groups was much higher than the control polystyrene plastic (more than 100 folds), with the i-BMP-2 group displaying slightly lower expression than the soluble BMP-2. Concurrently, Col-I and Runx2 groups' mRNA expression showed similar trends for all time points.

However, the mRNA expression of OCN of PGMA-BMP-2 was higher than BMP-2 solution in day 3 and day 5. From the results, we can see that PGMA-BMP-2 has less influence on ALP and Col-I than BMP-2 solution, which may be related to the activity of i-BMP-2 being marginally lower than that of free BMP-2 in solution. However, PGMA-BMP-2 is found to significantly enhance the mRNA expression level of OCN, seemingly because the i-BMP-2 is in tighter contact with BMP-2 receptors on the cell membrane surface for longer period of time.

3.6. Bioactivity of polymer brush-immobilized BMP-2 in vivo

The osteogenesis effectiveness of the produced scaffolds was investigated using a rat cranial critical-sized defect model in light of the bioactivity of polymer brush-immobilized BMP-2 *in vivo*. As shown in the high-resolution SRμCT and X-ray images (Fig. 6a), the implanted 3D printed scaffolds can be observed in all samples and the scaffolds with BMP-2 were integrated with the surrounding bone tissues at 6 weeks. It was shown that at 12 weeks, all the scaffolds were almost completely degraded. Quantitative results from SRμCT indicated that the new bone volume/tissue volume (BV/TV) of PGS/β-TCP-PGMA scaffolds were higher than those of PGS/β-TCP scaffolds (Fig. 6b). We inferred that the PGMA polymer brush might be more conducive to the adhesion of osteogenesis-related cells *in vivo* and accelerate the related osteogenesis process. The osteogenic effect of PGS/β-TCP-PGMA-BMP-2 scaffolds was markedly better than that of PGS/β-TCP-BMP-2 scaffolds at 6 and 12 weeks. Furthermore, we found that the osteogenesis of the PGS/β-TCP-PGMA-BMP-2 scaffolds was relatively uniform, while the PGS/β-TCP-BMP-2 scaffolds only repaired part of the defect area. We believe that this may be due to the easy loss of BMP-2 on the PGS/β-TCP-BMP-2 scaffolds, resulting in the absence of BMP-2 in some regions. Statistics data showed that the BV/TV and Tb.Th of PGS/β-TCP-PGMA-BMP-2 scaffolds were about 20%–50% higher than those of PGS/β-TCP-BMP-2 scaffolds at 6 and 12 weeks, respectively (Fig. 6b & c). It was showed that materials containing BMP-2 could significantly promote osteogenesis after implantation at bone defect sites, but this was related to the activity of BMP-2 on the materials [40]. The results proved that the PGMA brush-immobilized BMP-2 not only maintained the bioactivity of BMP-2 *in vivo*, but also had a longer-lasting effect and better osteogenic effect.

3.7. Histological and immunohistochemistry analysis

Subsequently, histological and immunohistochemistry analysis were carried out to further verify the osteogenic effect of the scaffolds. We found that, in Masson's Trichrome staining (Fig. 7), none of the scaffolds lacking BMP-2 had obvious new bone formation, but only a large amount of fibrous tissue and undegraded material. The new bone formed around the PGS/β-TCP-PGMA-BMP-2 scaffolds was relatively uniform. Although there was still more undegraded material at 6 weeks, the new bone was obviously connected into one piece. In contrast, PGS/β-TCP-BMP-2 scaffolds showed nonunion at 6 and 12 weeks. These results further indicated that the PGMA brush-immobilized BMP-2 had better osteogenesis effect. From Fig. 8a, we can see that at 6 and 12 weeks, PGS/β-TCP-PGMA-BMP-2 scaffolds had significantly more OCN (osteogenesis marker, brown area) than the PGS/β-TCP-BMP-2 scaffolds, and the scaffolds without BMP-2. From the results of CD31 (angiogenesis marker, Fig. 8b), we can see that at 6 weeks, the angiogenic capacity of the PGS/β-TCP-PGMA-BMP-2 scaffolds was the best. At 12 weeks, the content of CD31 in all 4 stents decreased, which may be due to the decreased activity of angiogenic activity at the later stage of repair. TRAP is a lysosomal enzyme released by osteoclasts [41]. We believe that osteoclasts are important participating cells in the process of bone remodeling. It was showed that the two scaffolds containing BMP-2 had high osteoclast activity at 6 weeks from the TRAP staining results (Fig. 8c), and the PGS/β-TCP-PGMA-BMP-2 induced the highest amount of $TRAP^{+}$ osteoclasts relative to other groups at 6 weeks. Previous studies have confirmed that BMP-2 can significantly promote the osteogenesis process at the bone defect site at an early stage, and at the same time enhance the bone resorption of osteoclasts, accelerating the

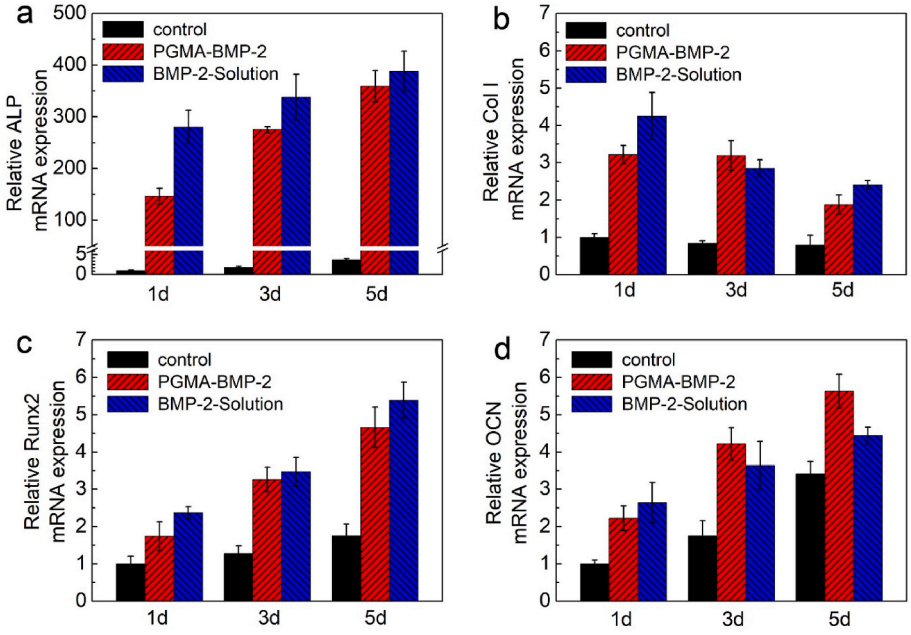

Fig. 5. Effect of PGMA-BMP-2 and free BMP-2 in solution on the expression of osteogenic marker gene ALP (a), Col-I (b), Runx2 (c) and OCN (d) in C2C12 cells cultured at day 1, 3 and 5 by real-time RT-PCR. The amount of BMP-2 in solution and immobilized on the PGMA polymer brushes is 1.35 μg.

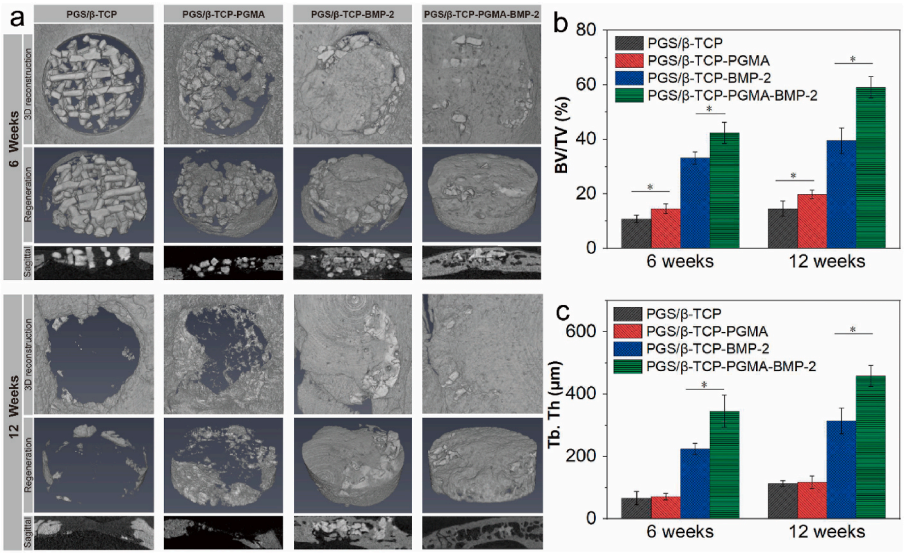

Fig. 6. Bone-tissue regeneration within rat cranial defect model after 6-week and 12-week implantation of PGS/β-TCP scaffolds, PGS/β-TCP-PGMA scaffolds, PGS/β-TCP-BMP-2 scaffolds and PGS/β-TCP-PGMA-BMP-2 scaffolds. (a) High-resolution SRμCT reconstruction images of 3D reconstruction, regeneration area and sagittal sections of defect area after 6 weeks and 12 weeks of regeneration. SRμCT quantification of (b) the bone volume/total volume (BV/TV) and (c) trabecular thickness (Tb.Th) in defect area. (*p < 0.05).

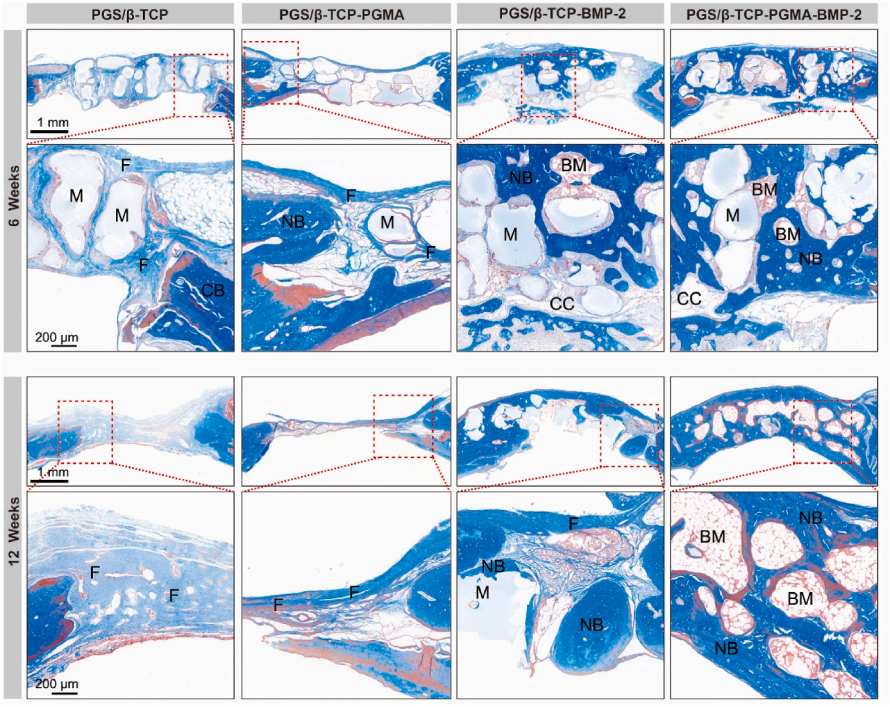

Fig. 7. Histological evaluation of bone regeneration sections at 6 weeks and 12 weeks by Masson's trichrome staining. (NB: new bone; CB: cancellous bone; F: fibrous tissue; M: materials; BM: bone marrow; CC: cartilage).

process of bone remodeling [14]. It was demonstrated that the PGS/β-TCP-PGMA-BMP-2 scaffolds could provide a better microenvironment for osteoclastogenesis as well as bone remodeling relative to other groups. This also proves that the PGMA brush-immobilized BMP-2 has better osteogenic effect *in vivo*. Of note, it was found that there was a large number of osteoclasts around the undegraded material at 6 weeks, indicating that osteoclasts could significantly promote the degradation of the material. At 12 weeks, the material was almost degraded, and BMP-2 did not continue to remain at the site, and the activity of osteoclasts was significantly decreased.

The above *in vitro* results showed that the i-BMP-2 with PGMA polymer brushes could maintain the bioactivity of BMP-2. Same as BMP-2 in solution, PGMA-BMP-2 could bind to its specific cell surface receptors immediately to activate the downstream Smad signaling pathway and result in enhanced osteogenic differentiation (Fig. 9).

4. Conclusion

In summary, we have successfully fabricated homogeneous PGMA polymer brushes onto the surface of various tissue engineering platforms (Au substrate, quartz glass, silica wafer, PCL and PMMA) with SI-ATRP. We found that the PGMA polymer brushes exhibit great capacity to bind BMP-2 and maintain its bioactivity *in vitro* and *in vivo*. BMP-2 could be covalently immobilized onto the surface of PGMA by coupling amine functional groups of BMP-2 to PGMA reactive epoxy groups via a ring-opening reaction. The i-BMP-2 could lead to differentiation of the

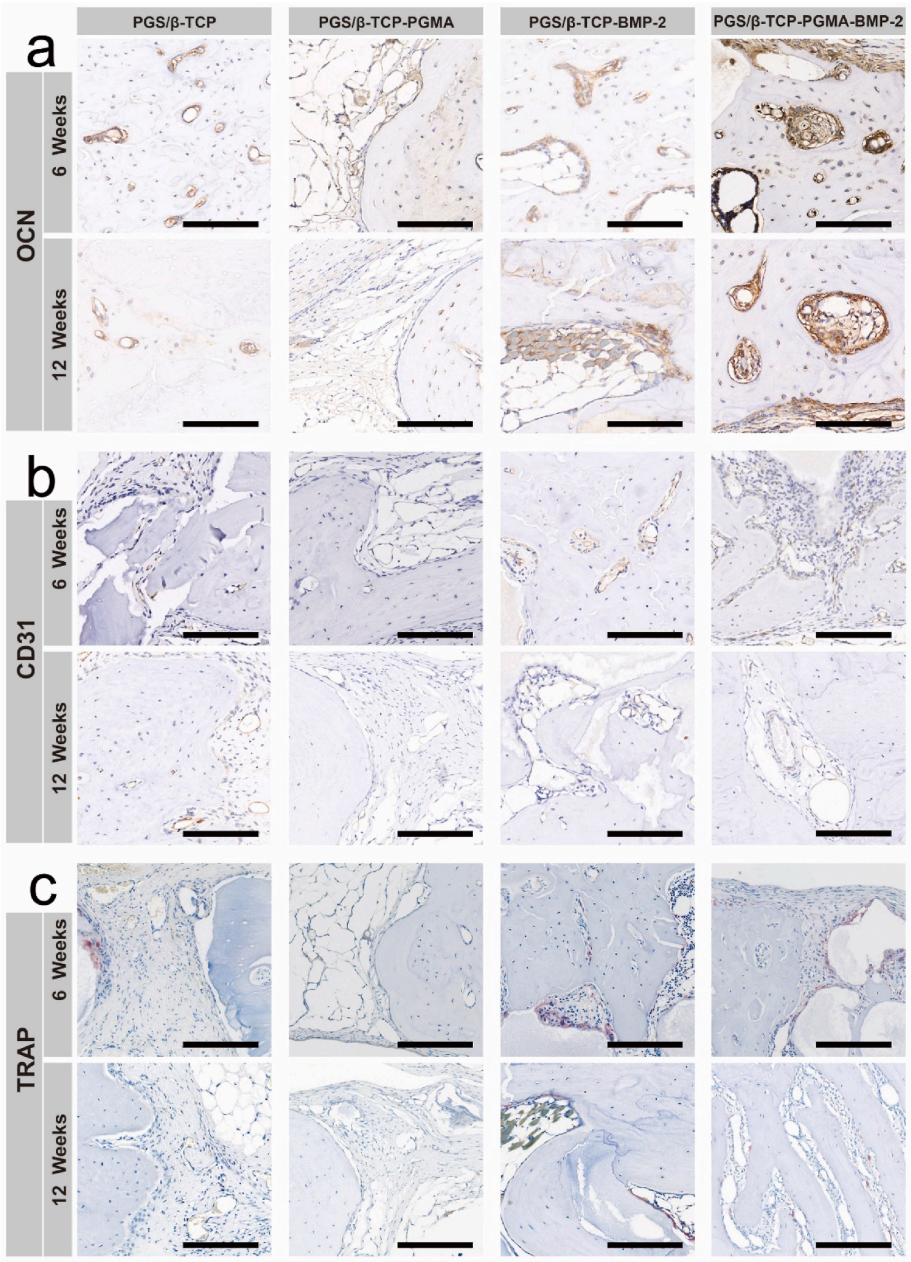

Fig. 8. Immunohistochemical staining of (a) osteogenic-related protein OCN, (b) angiogenic-related protein CD31 and (c) TRAP after implantation for 6 weeks and 12 weeks. (scale bar: 200 μm).

myoblastic precursor cells along the osteoblastic lineage, with excellent bioactivity (up to 87% bioactivity of free BMP-2). The bioactivity is maintained as covalent immobilization will not disrupt the conformation of BMP-2 and the internal substructure of α-helix and β-sheets. Moreover, with the PGMA-PNIPAm binary polymer brushes, the immobilization of BMP-2 by PGMA nanopatterns reveal a much better osteogenic activity (up to 110% bioactivity of free BMP-2). In our animal experiments with cranial critical-sized defect model, PGMA brush-immobilized BMP-2 showed better osteogenic effect than the adsorbed BMP-2 *in vivo*. Notably, the method for creating *in-situ* BMP-2 binding to biomaterial surfaces is significantly advantageous since BMP-2 could be binding to the surfaces of plenty of tissue engineering materials and our technique could be used to study other active growth factors. We believe that our covalent immobilization strategy could be applicable for locally controlling biomacromolecule conjugation, thereby accelerating regeneration of a variety of tissue types, for example, bone and cartilage repair.

CRediT authors contribution statement

Zijian Zheng conceived, designed and supervised the project; Qi Gan conducted the synthesis and biological characterization; Lina Chen performed part of the nanoline sample; Ho-Pan Bei revised the manuscript; Sze-Wing Ng performed the Raman characterization; Han Guo performed the synchrotron radiation-based μCT analyses; Guoqiang Liu and Hao Pan provided some useful suggestions; Qi Gan and Xin Zhao wrote the manuscript. Zijian Zheng, Changsheng Liu and Xin Zhao provided resources.

Declaration of competing interest

The authors declare that they have no known competing financial interests or personal relationships that could have appeared to influence the work reported in this paper.

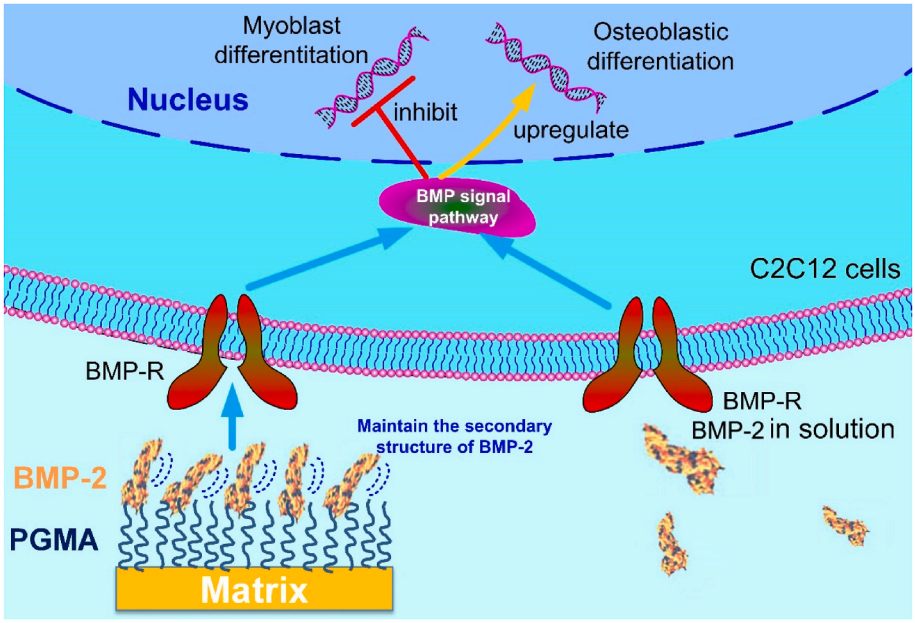

Fig. 9. Proposed mechanism of PGMA-immobilized BMP-2 (i-BMP-2) and free BMP-2 in solution on osteoblast differentiation. The i-BMP-2 could activate the downstream Smad signaling by binding to specific cell surface BMP receptors, same as free BMP-2 in solution.

Acknowledgments

The authors declare no conflict of interest. Zijian Zheng acknowledges financial support from RGC Senior Research Fellow Scheme (SRFS2122-5S04), Research Grants Council of Hong Kong. Xin Zhao acknowledges Collaborative Research Fund (C5044-21GF) from the Research Grants Council of Hong Kong and National Excellent Young Scientists Fund (Hong Kong and Macau, 82122002), National Natural Science Foundation of China. Qi Gan acknowledges support from National Natural Science Foundation of China (No. 32071337) and Shanghai Pujiang Program (20PJ1402600).

Appendix A. Supplementary data

Supplementary data to this article can be found online at https://doi.org/10.1016/j.bioactmat.2022.12.029.

References

[1] L. Cheng, X. Sun, X. Zhao, L. Wang, J. Yu, G. Pan, B. Li, H. Yang, Y. Zhang, W. Cui, Surface biofunctional drug-loaded electrospun fibrous scaffolds for comprehensive repairing hypertrophic scars, Biomaterials 83 (2016) 169–181.
[2] D. Chen, M. Zhao, G.R. Mundy, Bone morphogenetic proteins, Growth Factors 22 (2004) 233–241.
[3] A.W. Yasko, J.M. Lane, E.J. Fellinger, V. Rosen, J.M. Wozney, E.A. Wang, The healing of segmental bone defects, induced by recombinant human bone morphogenetic protein (rhBMP-2). A radiographic, histological, and biomechanical study in rats, J. Bone Joint Surg. Am. 74A (1992) 659–670.
[4] E.A. Wang, V. Rosen, J.S. Dalessandro, M. Bauduy, P. Cordes, T. Harada, D.I. Israel, R.M. Hewick, K.M. Kerns, P. Lapan, D.P. Luxenberg, D. McQuaid, I.K. Moutsatsos, J. Nove, J.M. Wozney, Recombinant human bone morphogenetic protein induces bone formation, P. Natl. Acad. Sci. USA 87 (1990) 2220–2224.
[5] E. Gazzerro, E. Canalis, Bone morphogenetic proteins and their antagonists, Rev. Endocr. Metab. Disord. 7 (2006) 51–65.
[6] J.M. Wozney, V. Rosen, A.J. Celeste, L.M. Mitsock, M.J. Whitters, R.W. Kriz, R. M. Hewick, E.A. Wang, Novel regulators of bone formation: molecular clones and activities, Science 242 (1988) 1528–1534.
[7] H.J. Cho, S.K.M. Perikamana, J.H. Lee, J. Lee, K.M. Lee, C.S. Shin, H. Shin, Effective immobilization of BMP-2 mediated by polydopamine coating on biodegradable nanofibers for enhanced in vivo bone formation, ACS Appl. Mater. Interfaces 6 (2014) 11225–11235.
[8] S.K. Boda, Y. Almoshari, H.J. Wang, X.Y. Wang, R.A. Reinhardt, B. Duan, D. Wang, J.W. Xie, Mineralized nanofiber segments coupled with calcium-binding BMP-2 peptides for alveolar bone regeneration, Acta Biomater. 85 (2019) 282–293.
[9] B.B. Seo, J.T. Koh, S.C. Song, Tuning physical properties and BMP-2 release rates of injectable hydrogel systems for an optimal bone regeneration effect, Biomaterials 122 (2017) 91–104.
[10] X. Zhao, S. Liu, L. Yildirimer, H. Zhao, R. Ding, H. Wang, W. Cui, D. Weitz, Injectable stem cell-laden photocrosslinkable microspheres fabricated using microfluidics for rapid generation of osteogenic tissue constructs, Adv. Funct. Mater. 26 (2016) 2809–2819.
[11] Y. Yang, Q. Zhang, T. Xu, H. Zhang, M. Zhang, L. Lu, Y. Hao, J.Y.H. Fuh, X. Zhao, Photocrosslinkable nanocomposite ink for printing strong, biodegradable and bioactive bone graft, Biomaterials 263 (2020), 120378.
[12] Q. Fan, J. Bai, H. Shan, Z. Fei, H. Chen, J. Xu, Q. Ma, X. Zhou, C. Wang, Implantable blood clot loaded with BMP-2 for regulation of osteoimmunology and enhancement of bone repair, Bioact. Mater. 6 (2021) 4014–4026.
[13] B. Huang, Z. Wu, S. Ding, Y. Yuan, C. Liu, Localization and promotion of recombinant human bone morphogenetic protein-2 bioactivity on extracellular matrix mimetic chondroitin sulfate-functionalized calcium phosphate cement scaffolds, Acta Biomater. 71 (2018) 184–199.
[14] Y. Yu, R. Chen, Y. Yuan, J. Wang, C. Liu, Affinity-selected polysaccharide for rhBMP-2-induced osteogenesis via BMP receptor activation, Appl. Mater. Today 20 (2020), 100681.
[15] M.M. Martino, P.S. Briquez, A. Ranga, M.P. Lutolf, J.A. Hubbell, Heparin-binding domain of fibrin(ogen) binds growth factors and promotes tissue repair when incorporated within a synthetic matrix, P. Natl. Acad. Sci. USA 110 (2013) 4563–4568.
[16] S.S. Lee, T. Fyrner, F. Chen, Z. Alvarez, E. Sleep, D.S. Chun, J.A. Weiner, R. W. Cook, R.D. Freshman, M.S. Schallmo, K.M. Katchko, A.D. Schneider, J.T. Smith, C.W. Yun, G. Singh, S.Z. Hashmi, M.T. McClendon, Z.L. Yu, S.R. Stock, W.K. Hsu, E. L. Hsu, S.I. Stupp, Sulfated glycopeptide nanostructures for multipotent protein activation, Nat. Nanotechnol. 12 (2017) 821. +.
[17] H.M. Xia, X. Li, W.W. Gao, X. Fu, R.H. Fang, L.F. Zhang, K. Zhang, Tissue repair and regeneration with endogenous stem cells, Nat. Rev. Mater. 3 (2018) 174–193.
[18] Z.M. Wang, Z.F. Wang, W.W. Lu, W.X. Zhen, D.Z. Yang, S.L. Peng, Novel biomaterial strategies for controlled growth factor delivery for biomedical applications, NPG Asia Mater. 9 (2017) e435.
[19] T. Crouzier, L. Fourel, T. Boudou, C. Albiges-Rizo, C. Picart, Presentation of BMP-2 from a soft biopolymeric film unveils its activity on cell adhesion and migration, Adv. Mater. 23 (2011) 111–118.
[20] D. Lin, Y.J. Chai, Y.F. Ma, B. Duan, Y. Yuan, C.S. Liu, Rapid initiation of guided bone regeneration driven by spatiotemporal delivery of IL-8 and BMP-2 from hierarchical MBG-based scaffold, Biomaterials 196 (2019) 122–137.
[21] B.R. Coad, M. Jasieniak, S.S. Griesser, H.J. Griesser, Controlled covalent surface immobilisation of proteins and peptides using plasma methods, Surf. Coating. Technol. 233 (2013) 169–177.
[22] W. Wang, L. Lu, H.P. Bei, X. Li, Z. Du, M.F. Maitz, N. Huang, Q. Tu, X. Zhao, Z. Yang, Self-protonating, plasma polymerized, superimposed multi-layered biomolecule nanoreservoir as blood-contacting surfaces, Chem. Eng. J. 410 (2021), 128313.
[23] L.N. Chen, Z. Xie, T.S. Gan, Y. Wang, G.Z. Zhang, C.A. Mirkin, Z.J. Zheng, Biomimicking nano-micro binary polymer brushes for smart cell orientation and adhesion control, Small 12 (2016) 3400. +.
[24] G. Liu, M. Hirtz, H. Fuchs, Z. Zheng, Development of Dip-Pen Nanolithography (DPN) and its derivatives, Small 15 (2019) 1900564.

[25] G. Liu, S.H. Petrosko, Z. Zheng, C.A. Mirkin, Evolution of Dip-Pen Nanolithography (DPN): from molecular patterning to materials discovery, Chem. Rev. 120 (2020) 6009–6047.
[26] G. Liu, M. Rong, H. Hu, L. Chen, Z. Xie, Z. Zheng, 3D Dip-Pen Nanolithography, Adv. Mater. Technol. 7 (2022) 2101493.
[27] Y. Ma, C. Zhang, Y. Wang, L. Zhang, J. Zhang, J. Shi, J. Si, Y. Yuan, C. Liu, Direct three-dimensional printing of a highly customized freestanding hyperelastic bioscaffold for complex craniomaxillofacial reconstruction, Chem. Eng. J. 411 (2021).
[28] K. Yang, J. Zhang, X. Ma, Y. Ma, C. Kan, H. Ma, Y. Li, Y. Yuan, C. Liu, beta-Tricalcium phosphate/poly(glycerol sebacate) scaffolds with robust mechanical property for bone tissue engineering, Mater. Sci. Eng. C-Mater. 56 (2015) 37–47.
[29] J.-I. Jung, K.-Y. Park, Y. Lee, M. Park, J. Kim, Vitamin C-linker-conjugated tripeptide AHK stimulates BMP-2-induced osteogenic differentiation of mouse myoblast C2C12 cells, Differentiation 101 (2018) 1–7.
[30] R. Nishimura, Y. Kato, D. Chen, S.E. Harris, G.R. Mundy, T. Yoneda, Smad5 and DPC4 are key molecules in mediating BMP-2-induced osteoblastic differentiation of the pluripotent mesenchymal precursor cell line C2C12, J. Biol. Chem. 273 (1998) 1872–1879.
[31] I.S. Kim, Y.M. Song, T.H. Cho, J.Y. Kim, F.E. Weber, S.J. Hwang, Synergistic action of static stretching and BMP-2 stimulation in the osteoblast differentiation of C2C12 myoblasts, J. Biomech. 42 (2009) 2721–2727.
[32] X. Chen, B. Tan, Z. Bao, S. Wang, R. Tang, Z. Wang, G. Chen, S. Chen, W.W. Lu, D. Yang, S. Peng, Enhanced bone regeneration via spatiotemporal and controlled delivery of a genetically engineered BMP-2 in a composite Hydrogel, Biomaterials 277 (2021), 121117.
[33] K. Hauff, C. Zambarda, M. Dietrich, M. Halbig, A.L. Grab, R. Medda, E. A. Cavalcanti-Adam, Matrix-immobilized BMP-2 on microcontact printed fibronectin as an in vitro tool to study BMP-mediated signaling and cell migration, Front. Bioeng. Biotechnol. 3 (2015) 62.
[34] Q. Gan, H. Pan, W. Zhang, Y. Yuan, J. Qian, C. Liu, Fabrication and evaluation of a BMP-2/dexamethasone co-loaded gelatin sponge scaffold for rapid bone regeneration, Regenerative Biomater. 9 (2022).
[35] T.L.M. Pohl, J.H. Boergermann, G.K. Schwaerzer, P. Knaus, E.A. Cavalcanti-Adam, Surface immobilization of bone morphogenetic protein 2 via a self-assembled monolayer formation induces cell differentiation, Acta Biomater. 8 (2012) 772–780.
[36] J. Cabanas-Danes, E. Landman, J. Huskens, M. Karperien, P. Jonkheijm, Hydrolytically labile linkers regulate release and activity of human bone morphogenetic protein-6, Langmuir 34 (2018) 9298–9306.
[37] G.A. Hudalla, W.L. Murphy, Biomaterials that regulate growth factor activity via bioinspired interactions, Adv. Funct. Mater. 21 (2011) 1754–1768.
[38] Z.F. Lin, M.M. Wu, H.M. He, Q.F. Liang, C.S. Hu, Z.W. Zeng, D.L. Cheng, G. C. Wang, D.F. Chen, H.B. Pan, C.S. Ruan, 3D printing of mechanically stable calcium-free alginate-based scaffolds with tunable surface charge to enable cell adhesion and facile biofunctionalization, Adv. Funct. Mater. 29 (2019), 1808439.
[39] J. Gaeanin, J. Hedrich, S. Sieste, G. Glasser, I. Lieberwirth, C. Schilling, S. Fischer, H. Barth, B. Knoll, C.V. Synatschke, T. Weil, Autonomous ultrafast self-healing hydrogels by pH-responsive functional nanofiber gelators as cell matrices, Adv. Mater. 31 (2019), 1805044.
[40] S. Liu, Y. Liu, L. Jiang, Z. Li, S. Lee, C. Liu, J. Wang, J. Zhang, Recombinant human BMP-2 accelerates the migration of bone marrow mesenchymal stem cells via the CDC42/PAK1/LIMK1 pathway in vitro and in vivo, Biomater. Sci. 7 (2019) 362–372.
[41] H. Xie, Z. Cui, L. Wang, Z. Xia, Y. Hu, L. Xian, C. Li, L. Xie, J. Crane, M. Wan, G. Zhen, Q. Bian, B. Yu, W. Chang, T. Qiu, M. Pickarski, D. Le Thi, J.J. Windle, X. Luo, E. Liao, X. Cao, PDGF-BB secreted by preosteoclasts induces angiogenesis during coupling with osteogenesis, Nat. Med. 20 (2014) 1270–1278.